Electrical Spin Injection and Detection in Silicon Nanowires through Oxide Tunnel Barriers
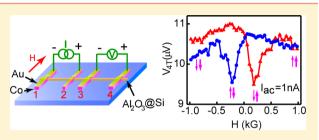
Shixiong Zhang,*[,†,‖] Shadi A. Dayeh,[†,⊥] Yan Li,[‡] Scott A. Crooker,[‡] Darryl L. Smith,[§] and S. T. Picraux*[,†]

[†]Center for Integrated Nanotechnologies, Los Alamos National Laboratory, Los Alamos, New Mexico 87545, United States
[‡]National High Magnetic Field Laboratory, Los Alamos National Laboratory, Los Alamos, New Mexico 87545, United States
[§]Theoretical Division, Los Alamos National Laboratory, Los Alamos, New Mexico 87545, United States

Ⓢ Supporting Information

ABSTRACT: We demonstrate all-electrical spin injection, transport, and detection in heavily n-type-doped Si nanowires using ferromagnetic Co/Al_2O_3 tunnel barrier contacts. Analysis of both local and nonlocal spin valve signals at 4 K on the same nanowire device using a standard spin-transport model suggests that high spin injection efficiency (up to ~30%) and long spin diffusion lengths (up to ~6 μm) are achieved. These values exceed those reported for spin transport devices based on comparably doped bulk Si. The spin valve signals are found to be strongly bias and temperature dependent and can invert sign with changes in the dc bias current. The influence of the nanowire morphology on field-dependent switching of the contacts is also discussed. Owing to their nanoscale geometry, ~5 orders of magnitude less current is required to achieve nonlocal spin valve voltages comparable to those attained in planar microscale spin transport devices, suggesting lower power consumption and the potential for applications of Si nanowires in nanospintronics.

KEYWORDS: Spintronics, spin injection, silicon nanowires, tunnel barrier

Silicon (Si) is arguably the most important material for today's semiconductor technologies. In the past decade, functional one-dimensional Si nanowire devices have been demonstrated for a wide variety of proof-of-concept nanoscale structures, including nanowire transistors,[1] photon detectors,[2] and solar cells.[3,4] The successful integration of these nanowire devices into large area architectures has brought new opportunities for commercialization.[5−7] However, to date most of these nanowire devices exploit only the electron's charge degree of freedom. Adding the electron's spin degree of freedom to such charge-based electronics is believed to add substantially more capability and to improve performance,[8,9] e.g., nonvolatility, increased data processing speed, and decreased electric power consumption, which are of high demand in information technology applications.

Recently, significant progress has been made in semiconductor-based spin electronics. Using ferromagnetic electrodes as spin injectors and/or spin detectors, all-electrical spin injection,[10−12] spin transport,[10,11] spin detection,[10,11] and spin accumulation[13−15] have been realized in bulk silicon.[9] A wide variety of spin studies have also been performed in bulk germanium (Ge),[16] gallium arsenide (GaAs),[17−19] graphene,[20,21] and carbon nanotubes.[22,23] In comparison, only a few studies of the spintronic properties of one-dimensional inorganic semiconductor nanowires (NWs), e.g., Si,[24−26] Ge,[27] indium nitride (InN),[28] gallium nitride (GaN),[29] and silicide,[30] have been reported to date. Owing to their reduced scale and one-dimensional confinement, nanowires are anticipated to possess novel and useful physical properties for future

generations of spin-based nanoscale devices. Indeed, it has been demonstrated that spin relaxation in III−V semiconductors can be significantly suppressed by reducing the transport channel width;[31] this is attributed to the suppression of momentum-dependent Dyakonov−Perel (DP) spin dephasing in semiconductors lacking crystalline inversion symmetry.[32] In group IV semiconductors such as Si and Ge, the inversion symmetry of the diamond crystal lattice as well as time-reversal invariance guarantees spin degeneracy and eliminates DP spin scattering. Thus, very long spin lifetimes and spin diffusion lengths are anticipated. Interestingly, Ge NWs have recently been reported to exhibit extremely long spin diffusion lengths.[27] Compared to Ge, Si has an even lower atomic mass and weaker spin−orbit interaction which could result in even longer spin lifetimes and diffusion lengths. Given the importance of Si in semiconductor technology, it is therefore of particular interest to explore spin injection, spin transport, and spin detection in Si nanowires.

Previous efforts on spin injection into Si NWs utilized metal-on-Si Schottky barriers for spin-dependent tunneling of electrons from ferromagnetic electrodes.[24−26] Since the effective Schottky barrier height is generally pinned at about half the Si bandgap irrespective of the contact metal,[33] and since the barrier thickness depends on the doping profile in the

semiconductor, detailed control of the semiconductor surface doping is required in approaches using only Schottky barriers.[17,18] As a result, the window for efficient spin injection may be limited. Alternatively, in planar spin transport devices oxide tunnel barriers are known to be an important ingredient in many successful electrical spin injection/detection studies,[34,35] and the tunneling characteristics can be readily controlled by tuning the oxide thickness alone. Considering the above points, it is thus of interest to combine these three promising aspects—the material Si, oxide tunnel barriers for spin injection, and one-dimensional nanoscale structures—into a single investigation.

Here we demonstrate for the first time that efficient electrical spin injection and detection can be achieved in heavily n-type-doped Si NWs by using ferromagnetic electrical contacts incorporating an oxide tunnel barrier. Analysis of local (two terminal) and nonlocal (four terminal) spin valve signals taken on the same device suggests that high spin injection efficiencies of up to ~30% and long spin diffusion lengths of up to ~6 μm can be achieved. Moreover, because of their nanoscale size, nonlocal spin valve voltages comparable to those for previous planar devices can be achieved using ~10^5 times less injection current. Finally, we show that the ferromagnet/tunnel barrier/Si nanowire spin valve signals are strongly influenced by both bias current and temperature.

The n-type phosphorus-doped Si NWs were grown on Si (100) substrates in a cold-walled chemical vapor deposition (CVD) system via the Au-catalyzed vapor−liquid−solid (VLS) mechanism. Phosphorus doping was achieved by a gas flow of 20 sccm of 5000 ppm PH_3 in H_2 together with 250 sccm of 50% SiH_4 in H_2 at a total pressure of 3 Torr; the growth process consisted of 1.5 min for NW nucleation at 525 °C followed by 30 min for NW elongation at 500 °C. The Au colloid nanoparticles used as growth seeds had diameters of ~100 nm. The NW morphology and crystal structure were characterized by scanning electron microscopy (SEM) and high-resolution transmission electron microscopy (HR-TEM). As shown in Figure 1a, high yields of Si NWs with diameters of 100−200 nm were obtained. The wires have smooth surfaces as indicated in a typical high-magnification SEM image (left panel of Figure 1b). The growth was along the [111] direction, as determined by HR-TEM and selective area electron diffraction (right panels of Figure 1b).

Initial electrical characterization of the Si NWs was performed using devices with ohmic electrical contacts (i.e., without Al_2O_3 tunnel barriers) to determine the dopant concentration and uniformity along the NWs. These devices were fabricated on 200 nm thick silicon nitride films on Si substrates using electron beam lithography followed by electron beam metal deposition. Cobalt metal (~200 nm thick) was deposited on the NWs immediately after the removal of native oxide by dilute hydrogen fluoride (HF) etching. All Co electrodes were covered by a 30 nm thick Au capping layer to prevent postprocessing oxidation. The dopant uniformity was characterized through a series of two-terminal current−voltage (I−V) measurements on devices with multiple electrodes (inset of Figure 1c). Each segment has the same channel length of 3 μm. At the same drain-source voltage, the current only decreases by 25% from the NW base to the tip over a distance of 20 μm (Figure 1c), indicating that the doping concentration is nearly uniform along the wire axis. The contact resistance of these ohmically contacted devices was determined by a comparison of 2-terminal and 4-terminal I−V characteristics.
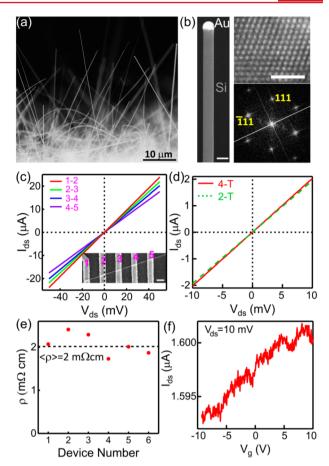

Figure 1. (a) A SEM image showing silicon NWs on growth substrate. (b) Left: a high-magnification SEM image near the tip of a Au-catalyzed Si NW; the scale bar is 150 nm. Upper right: a high-resolution TEM image showing two sets of {111} lattice fringes aligned with the NW growth direction; the scale bar is 2 nm. Lower right: the corresponding FFT pattern confirms a [111] growth direction. (c) Electrical characterizations of Si NWs using devices without tunneling contacts (ohmic Co contacts are deposited directly on the Si NW): Two-terminal I−V characteristics of a typical device; each segment has the same channel length. The scale bar in the SEM inset is 2 μm. (d) Two-terminal and four-terminal I−V are compared, indicating low-resistance ohmic contacts. (e) The resistivities of six Si NWs; the average resistivity is ~2 mΩ cm. (f) A typical gate-controlled channel current characteristic of a heavily doped Si nanowire device at a drain-to-source voltage of 10 mV, demonstrating n-type conductivity.

As seen in Figure 1d, these two I−V curves almost overlap with each other, and the contact resistance is found to be a few hundred ohms, which is an order of magnitude smaller than the typical resistance of each NW segment (~5 kΩ). The average resistivities of the NWs were found to be ~2 mΩ cm (Figure 1e), which corresponds to a dopant (phosphorus) concentration of 3×10^{19} cm^{-3} assuming bulk carrier mobilities. The heavily n-type-doped nature of these NWs is further confirmed by their gate response characteristics, i.e., the drain-source current increases only slightly with positive gate voltage (see Figure 1f).

The conductivity and spin lifetime mismatch between semiconductors (SC) and ferromagnetic metal (FM) electrodes is a major obstacle for efficient spin injection when using direct FM-on-SC contacts.[36] One of the most effective approaches for addressing this challenge is to insert a tunnel barrier at the SC/FM interface.[34,35] To achieve efficient spin injection into Si

NWs, we therefore deposited a thin conformal layer of Al_2O_3 (~0.5 nm as measured by HR-TEM) on the NW surface by atomic layer deposition immediately after the native oxide was removed by dilute HF etching. Then ferromagnetic Co/Au (200 nm/30 nm) contacts were deposited on the NWs. The tunneling nature of the contacts and the integrity of the thin Al_2O_3 layer was evidenced by their nonlinear $I-V$ characteristics (inset of Figure 2a) and by their temperature-dependent
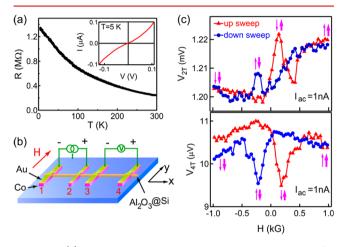

Figure 2. (a) Temperature-dependent two-terminal resistance of a silicon NW device having ferromagnetic $Co/Al_2O_3/Si$ tunneling contacts. Inset shows two-terminal $I-V$ characteristic at 5 K. (b) A schematic of the nonlocal spin transport measurement on a four-terminal spin-valve device. (c) Two-terminal (local; top panel) and four-terminal (nonlocal; bottom panel) spin valve signals plotted as ac voltages vs magnetic field H (the electrical current is $I = I_{dc} + I_{ac}$ with $I_{dc} = 10$ nA and $I_{ac} = 1$ nA). The two-terminal measurement was taken between electrodes 2 and 3, where the channel length between 2 and 3 is 1.6 μm, the NW diameter is 163 nm, and the widths of electrodes 2 and 3 are 400 and 700 nm, respectively.

resistance (Figure 2a).[37] The two-terminal resistance of the devices (~hundreds of kΩ at 300 K and ~1 MΩ at 5 K) is ~2 orders of magnitude larger than that of the NW itself (~5 kΩ), indicating that the oxide tunnel barrier contact resistance dominates.

We first performed spin transport measurements on Si NW devices (Figure 2b) in the local (two-terminal) configuration, where an electrical current was applied between two FM electrodes (E) 2 and 3, and the voltage drop V_{2T} between these two electrodes was measured as a function of the magnetic field H that was applied parallel to the long axis of the Co electrodes ($\pm y$; the magnetic easy axis of the electrodes). Electrical spin transport data were taken using a low-frequency (17 Hz) lock-in technique with $I_{dc} = 10$ nA and $I_{ac} = 1$ nA, where V_{2T} is the amplitude of the detected ac voltage. The upper panel of Figure 2c shows V_{2T} vs H of device 1, which has electrodes E2 and E3 of widths 400 and 700 nm, respectively, and a Si channel length of 1.6 μm. The Si nanowire diameter in this device is 163 nm. The two FM electrodes have different widths to provide different coercive fields; this was confirmed with magneto-optical Kerr rotation measurements on separate test samples of Co wire arrays. At $H = -0.98$ kG, the magnetization of contacts E2 and E3 are both aligned along $-y$. When the field is swept to ~+0.2 kG, the wider electrode E3 reverses its magnetization from $-y$ to $+y$ and becomes antiparallel to E2, generating an increase of V_{2T} (red curve of Figure 2c top panel). Upon further increasing H to ~+0.5 kG, the narrower contact E2 also

reverses its magnetization and becomes parallel to E3 once again, leading to a drop of V_{2T}. Sweeping H in the reverse direction results in a similar trace, reflected about $H = 0$.

Although these data exhibit the characteristic hallmarks of a real spin-valve effect, we note immediately that other phenomena such as local Hall effects[38] and/or magneto-Coloumb effects[39,40]—which have nothing to do with real spin injection and spin transport in the semiconductor channel—can give rise to very similar signals in two-terminal measurements. To examine whether our two-terminal (i.e., local) signals observed here are indeed associated with spin injection and spin transport, we performed nonlocal (four-terminal) electrical spin valve measurements. Nonlocal measurements are generally considered to be an important test to demonstrate spin injection/accumulation and spin transport in a semiconductor channel.[41] As shown in Figure 2b, an electrical current ($I_{dc} = 10$ nA and $I_{ac} = 1$ nA) is applied between the spin injector E2 and another electrode E1 that is placed further (~5 μm) away. Spin accumulation in the silicon NW under contact E2 is created by means of spin injection ($I_{dc} < 0$) or spin extraction ($I_{dc} > 0$) through E2. The net electron spin polarization in the Si nanowire diffuses from electrode E2 to E3 and is sensed by a voltage drop V_{4T} between the spin detector E3 (1.6 μm from E2) and a remote electrode E4 (~4.4 μm further away from E3). Again, we use low-frequency lock-in detection with $I_{dc} = 10$ nA and $I_{ac} = 1$ nA. The lower panel of Figure 2c shows a clear nonlocal spin-valve signal on the same device (device 1) that was used for the two-terminal measurements (upper panel). The spin-dependent difference ($\Delta V_{4T} = V_{\uparrow\uparrow} - V_{\uparrow\downarrow}$) between parallel and antiparallel alignments of E2 and E3 is the nonlocal voltage, which is ~1 μV in this device. A nonzero background signal is typically observed in four-terminal measurements and could be due to the leakage current between the contact and substrate or possibly to nonuniform electrical current injection at the contacts.[42] As seen in Figure 2c, the abrupt changes in ΔV_{4T} occur at approximately the same magnetic fields in local and nonlocal measurements. These nonlocal data therefore strongly suggest that some, if not all, of the two-terminal signals arise from real spin injection, transport, and detection in these Si NWs, rather than from potential artifacts mentioned above.

Applying a standard spin transport model[43−45] to these local and nonlocal data allows us to extract the two important spin-transport parameters relevant to these studies: spin diffusion length and spin injection efficiency. The magnitude of the voltage signals in the two- and four-terminal measurements are determined by the spin diffusion length, $\lambda_S = (D\tau_S)^{1/2}$ (where D is the electron diffusion constant and τ_S is the electron spin lifetime) and the contact spin injection efficiency $\Delta G/G$ (where ΔG is the difference and G is the sum of the contact tunneling conductances for spin-up and spin-down electrons). The two- and four-terminal measurements presented in Figure 2 were made using the same Si nanowire and the same set of contacts to the nanowire. Thus, from the magnitude of these signals it is possible to separately estimate these two parameters for this Si nanowire. Using standard models,[43−45] ΔV_{2T} and ΔV_{4T} can be expressed as

$$\Delta V_{2T} = C\left(\frac{4e^{-d/\lambda_S}}{1 - e^{-2d/\lambda_S}}\right) \quad \text{and} \quad \Delta V_{4T} = C\left(\frac{2e^{-\delta/\lambda_S}}{1 + e^{-2\delta/\lambda_S}}\right)$$

(1)

where

$$C = \frac{J}{A}\left(\frac{\Delta G}{G}\right)^2 \frac{\lambda_S}{neD}\left(\frac{4\varepsilon_F}{3e}\right)$$

Here, d is the spacing between the injecting and collecting contact in two-terminal measurements, δ is the spacing between injecting and detecting contact in four-terminal measurements ($d = \delta$ for the data in Figure 2), J is the ac current, A is the nanowire cross-sectional area, n is the electron density in the nanowire, e is the electron charge, and ε_F is the electron Fermi energy in the nanowire. The ratio $\Delta V_{2T}/\Delta V_{4T}$ therefore depends only on λ_S and not on $\Delta G/G$: $\Delta V_{2T}/\Delta V_{4T} = 2(1 + e^{-2d/\lambda_S})/(1 - e^{-2d/\lambda_S})$. Once λ_S is determined, either ΔV_{2T} or ΔV_{4T} can be used to estimate $\Delta G/G$.

If the two-terminal signal shown in Figure 2 is due entirely to spin-dependent transport (i.e., no contribution from local Hall or magneto-Coulomb effects), then $\Delta V_{2T} = 8\ \mu V$. Along with $\Delta V_{4T} = 1\ \mu V$ and the known values for the other parameters of the nanowire, we obtain $\lambda_S = (D\tau_S)^{1/2} \sim 6\ \mu m$ and $\Delta G/G \sim 30\%$. For electron-doped Si with $n \sim 3 \times 10^{19}$ cm^{-3}, D is ~ 4.35 cm^2/s and hence the spin lifetime $\tau_S \sim 90$ ns. For completeness, however, we also point out that if the two-terminal signal arises only partially from spin injection as discussed earlier or, for example, contact geometry effects lead to larger signals than expected in the simple model, then our estimates of the spin diffusion length and spin injection efficiency must be revised. Interestingly, however, the revised values are modified in opposite directions. For example, if only half of the two-terminal signal arises from real spin injection and transport, then the extracted spin diffusion length decreases to $\sim 3\ \mu m$, but the spin injection efficiency increases to $\sim 45\%$.

The spin injection efficiency and spin diffusion length (spin lifetime) in our nanowire device are comparable with or even higher than the $\sim 2\ \mu m$ lengths found in planar Si devices with comparable n-type doping.[11] This suggests that spin relaxation due to surface scattering is not substantially increased in NW devices, even though the surface scattering is enhanced in NWs due to the increased surface-area-to-volume ratio.[46] We note that highly doped (5×10^{19} cm^{-3}) Ge nanowires were recently inferred to have spin diffusion lengths of $\sim 100\ \mu m$[27] based on analysis of the contact resistance window over which spin injection was observed, and this value is much longer than was obtained in planar Ge even with light doping (2×10^{16} cm^{-3}).[16] Since the spin–orbit interaction in silicon is weaker than in germanium, the much shorter spin diffusion length inferred in our Si NWs compared to that inferred from Ge NWs[27] using a different analysis approach is unexpected. These results highlight the need for careful and systematic studies of spin transport in both silicon and germanium nanowires as a function of contact spacing and also for precession-dependent (Hanle effect) studies as an independent measure of spin lifetimes and diffusion constants.

We now compare the nonlocal spin valve signals in our nanodevices with the ones achieved in bulk Si microdevices with similar doping concentration and channel length. To obtain the same magnitude of signal ($\sim 1\ \mu V$),[11] the injection current to the microdevices has to be >100 μA, while only ~ 1 nA is needed in our NW devices. Thus, significantly lower injection currents, or correspondingly higher signal voltages, can be achieved in nanowire spin devices. This low injection current is because of both the small cross-sectional area and the high spin injection and long diffusion lengths in our NW devices. The electrical power consumption is $P = I^2 R = J^2 A\rho l$, where ρ is the resistivity of the nanowire and R and l are the

resistance and length of the nanowire segment between the electrodes 1 and 2 (Figure 2b), respectively. In order to generate the same amount of spin-valve signal, the same current density J is required. So the much smaller cross-sectional area A of nanowires compared to microscale devices suggests that the electrical power consumption of spin-valve devices may be decreased in nanodevices.

The magnetic-field-dependent switching of the voltage in our Si NW spin valve devices (and also in the previously reported Ge NW devices[27]) is not as sharp as in planar devices.[11,16,17,20,21] This may be due to the cylindrical morphology of the ferromagnetic Co electrodes on the NW. As shown in a typical SEM image (Figure 3a), the cobalt contact is buckled on
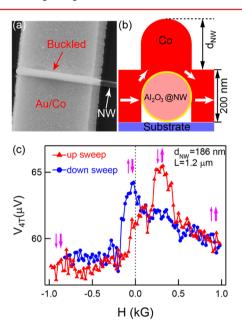

Figure 3. (a) A SEM image of the Au/Co contact (top view, slightly tilted). (b) A schematic of the cross section of the contact on the NW (Au is not shown); d_{NW} corresponds to the diameter of the Al$_2$O$_3$-covered Si NW. (c) The four-terminal spin-valve signal of a Si NW device with a diameter of 186 nm and channel length of 1.2 μm ($I_{dc} = 10$ nA, $I_{ac} = 1$ nA, and $T = 4$ K).

top of the Si NW. This contact morphology does not allow for a smooth planar interface with a well-defined magnetization orientation and can create local domain fluctuations. The region (Figure 3b) between the buckled and planar segments may have a FM easy axis that is not aligned with H. Since the height of the buckled segment equals to the nanowire diameter, this effect should be more pronounced in bigger nanowires (given the same cobalt thickness). Figure 3c shows the spin valve signal for a nanowire with a larger diameter of 186 nm. The transition from parallel to antiparallel contact magnetization during up- or down-sweep of H is slightly broader than that of the smaller nanowire (~ 163 nm) in Figure 2c. For example, in the up-sweep of H, the transition from parallel to antiparallel occurs from ~ 0 to ~ 0.2 kG for the 163 nm NW but occurs from ~ -0.2 to 0.25 kG for the 186 nm NW (Figure 3c); the transition from antiparallel back to parallel occurs from ~ 0.2 to 0.6 kG for the former but occurs from ~ 0.32 to above 1 kG for the latter. It appears that in order to force two FM electrodes for the 186 nm NW to fully parallel to each other (Figure 3c), a magnetic field higher than 1 kG (beyond the limitation of our instrument) is required. This nonsaturation of

magnetization is likely to be the reason for asymmetry between up-sweep and down-sweep curves. Moreover, the fact that the transition begins before H reaches zero is likely because with the decrease of field (from either direction) to zero, part of the contacts' magnetization rotates away from the applied field direction leading to a more gradual change of the nonlocal voltage. The effect of FM contacts wrapping around a nanowire and its influence on spin valve data is supported by a recent detailed study of such effects for InN nanowires.[28] In that study an intermediate fill layer was used to increase the planarity of the ferromagnetic contact to the nanowire, demonstrating the reduction in such magnetic anisotropy effects as a more planar structure is approached. We also noted that the background of the signal in Figure 3c is larger than that in Figure 2c, which may be due to a higher leakage current between the contact and substrate or more nonuniform electrical current injection at the contacts.[42]

Another interesting feature in Figure 3c is the inverted sign of the nonlocal signal (ΔV_{4T}); i.e., a larger voltage in the antiparallel configuration is observed, in contrast to the data shown in Figure 2. This situation can arise if the injection and detection electrodes have spin-dependent tunneling efficiencies of opposite sign. This situation has been shown to arise in nonlocal studies of planar Fe/GaAs devices[17,47] and also in all-metallic spin valves; its origin is a strongly *bias dependent* spin injection efficiency $\Delta G/G$,[48,49] which can switch sign depending on the electrical bias across the ferromagnet/semiconductor contact. In our nonlocal measurements, the detector E3 operates at zero bias, in contrast to the biased injector E2 ($I_{dc} = 10$ nA); therefore, it is possible that $\Delta G/G$ of E2 and E3 have different signs, leading to a nonlocal voltage ΔV_{4T} of inverted sign. To test this scenario, we measured ΔV_{4T} as a function of the dc electrical bias (bias current) across the injection contact E2 on another device showing similar behavior. As seen in Figure 4a, for increasing positive dc biases ($I_{dc} > 0$, extraction), ΔV_{4T} drops quickly and reaches a negative value at $I_{dc} = 20$ nA. For negative dc biases ($I_{dc} < 0$, injection),

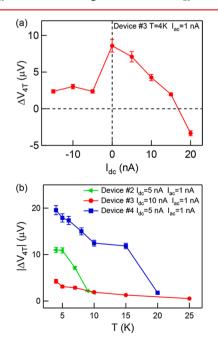ΔV_{4T} is reduced but does not show a strong bias dependence. The bias-dependent spin valve signal observed here indeed suggests that spin-injection efficiency can be strongly influenced by the electrical bias across the $Co/Al_2O_3/Si$ tunnel barrier.

We have also studied the temperature dependence of the spin valve signals for our Si nanowires. Figure 4b shows data taken on devices 2, 3, and 4. For all these devices, ΔV_{4T} decreases rapidly with increasing temperature and approaches zero at ~25 K, which is qualitatively consistent with previous reports of spin transport in planar Si devices.[12] According to eq 1, the reduction of ΔV_{4T} could be due to either a decrease of $\Delta G/G$ or λ_S. We note that the nonlocal spin signal of a Fe/GaAs device was also observed to decrease significantly with increasing temperature and attributed to the dramatic decrease of spin lifetime.[50] However, nonlocal Hanle measurements in highly doped ($n \sim 10^{19}$ cm^{-3}) bulk n-Si have shown that the spin lifetime and spin diffusion length do not change significantly with temperature from 8 to 150 K.[11] If this is also true in our NWs, then the rapid decrease of ΔV_{4T} with increased temperature should be attributed to a reduction of $\Delta G/G$. In this case, it may be possible to achieve spin-valve effects at higher temperatures through careful attention to the design and fabrication of high quality interface structures.

In summary, we have demonstrated for the first time that efficient electrical spin injection and detection in n-type Si NWs can be obtained through the use of oxide tunnel barriers grown by atomic layer deposition. The analysis of local and nonlocal spin valve signals on the same device using standard spin diffusion models suggests high spin injection efficiencies of up to ~30% and long spin diffusion lengths of up to ~6 μm, in contrast to ~2 μm in comparably doped bulk silicon. We also demonstrate that the spin valve signals can be strongly influenced by temperature, by bias current, and by the detailed morphology of the ferromagnetic electrodes. Because of their nanometer scale size, the nonlocal spin valve signals of NW devices require many orders of magnitude lower injection currents for comparable electrical signals compared to previous planar microscale spin devices, thus suggesting lower power consumption and the potential for applications of Si NWs in nanospintronics.

■ ASSOCIATED CONTENT

Ⓢ Supporting Information

Figures illustrating the reproducibility of the nonlocal spin valve measurements. This material is available free of charge via the Internet at http://pubs.acs.org.

■ AUTHOR INFORMATION

Corresponding Author

*E-mail: sxzhang@indiana.edu (S.X.Z.); picraux@lanl.gov (S.T.P.).

Present Addresses

‖Department of Physics, Indiana University, Bloomington, IN 47405.
⊥Department of Electrical and Computer Engineering, University of California, San Diego, La Jolla, CA 92092.

Notes

The authors declare no competing financial interest.

Figure 4. The ac nonlocal spin-valve voltages as functions of (a) dc bias current, I_{dc}, and (b) temperature, T.

■ REFERENCES

(1) Cui, Y.; Lieber, C. M. *Science* **2001**, *291*, 851−853.

(2) Hayden, O.; Agarwal, R.; Lieber, C. M. *Nat. Mater.* **2006**, *5*, 352−356.

(3) Picraux, S. T.; Yoo, J.; Campbell, I. H.; Dayeh, S. A.; Perea, D. E. In *Semiconductor Nanostructures for Optoelectronic Devices*; Gyu-Chul, Y., Ed.; Springer: New York, 2012; pp 297−328.

(4) Kelzenberg, M. D.; Boettcher, S. W.; Petykiewicz, J. A.; Turner-Evans, D. B.; Putnam, M. C.; Warren, E. L.; Spurgeon, J. M.; Briggs, R. M.; Lewis, N. S.; Atwater, H. A. *Nat. Mater.* **2010**, *9*, 239−244.

(5) Yan, H.; Choe, H. S.; Nam, S. W.; Hu, Y. J.; Das, S.; Klemic, J. F.; Ellenbogen, J. C.; Lieber, C. M. *Nature* **2011**, *470*, 240−244.

(6) Li, M. W.; Bhiladvala, R. B.; Morrow, T. J.; Sioss, J. A.; Lew, K. K.; Redwing, J. M.; Keating, C. D.; Mayer, T. S. *Nat. Nanotechnol.* **2008**, *3*, 88−92.

(7) Nam, S.; Jiang, X. C.; Xiong, Q. H.; Ham, D.; Lieber, C. M. *Proc. Natl. Acad. Sci. U. S. A.* **2009**, *106*, 21035−21038.

(8) Wolf, S. A.; Awschalom, D. D.; Buhrman, R. A.; Daughton, J. M.; von Molnar, S.; Roukes, M. L.; Chtchelkanova, A. Y.; Treger, D. M. *Science* **2001**, *294*, 1488−1495.

(9) Jansen, R. *Nat. Mater.* **2012**, *11*, 400−408.

(10) Appelbaum, I.; Huang, B. Q.; Monsma, D. J. *Nature* **2007**, *447*, 295−298.

(11) Sasaki, T.; Oikawa, T.; Suzuki, T.; Shiraishi, M.; Suzuki, Y.; Noguchi, K. *Appl. Phys. Lett.* **2010**, *96*, 122101.

(12) Ando, Y.; Hamaya, K.; Kasahara, K.; Kishi, Y.; Ueda, K.; Sawano, K.; Sadoh, T.; Miyao, M. *Appl. Phys. Lett.* **2009**, *94*, 182105.

(13) Dash, S. P.; Sharma, S.; Patel, R. S.; de Jong, M. P.; Jansen, R. *Nature* **2009**, *462*, 491−494.

(14) Gray, N. W.; Tiwari, A. *Appl. Phys. Lett.* **2011**, *98*, 102112.

(15) Li, C. H.; van't Erve, O. M. J.; Jonker, B. T. *Nat. Commun.* **2011**, *2*, 1256.

(16) Zhou, Y.; Han, W.; Chang, L. T.; Xiu, F. X.; Wang, M. S.; Oehme, M.; Fischer, I. A.; Schulze, J.; Kawakami, R. K.; Wang, K. L. *Phys. Rev. B* **2011**, *84*, 125323.

(17) Lou, X. H.; Adelmann, C.; Crooker, S. A.; Garlid, E. S.; Zhang, J.; Reddy, K. S. M.; Flexner, S. D.; Palmstrom, C. J.; Crowell, P. A. *Nat. Phys.* **2007**, *3*, 197−202.

(18) Lou, X.; Adelmann, C.; Furis, M.; Crooker, S. A.; Palmstrom, C. J.; Crowell, P. A. *Phys. Rev. Lett.* **2006**, *96*, 176603.

(19) Ciorga, M.; Einwanger, A.; Wurstbauer, U.; Schuh, D.; Wegscheider, W.; Weiss, D. *Phys. Rev. B* **2009**, *79*, 165321.

(20) Tombros, N.; Jozsa, C.; Popinciuc, M.; Jonkman, H. T.; van Wees, B. J. *Nature* **2007**, *448*, 571.

(21) Han, W.; Wang, W. H.; Pi, K.; McCreary, K. M.; Bao, W.; Li, Y.; Miao, F.; Lau, C. N.; Kawakami, R. K. *Phys. Rev. Lett.* **2009**, *102*, 137205.

(22) Tsukagoshi, K.; Alphenaar, B. W.; Ago, H. *Nature* **1999**, *401*, 572−574.

(23) Sahoo, S.; Kontos, T.; Furer, J.; Hoffmann, C.; Graber, M.; Cottet, A.; Schonenberger, C. *Nat. Phys.* **2005**, *1*, 99−102.

(24) Lin, Y. C.; Chen, Y.; Shaios, A.; Huang, Y. *Nano Lett.* **2010**, *10*, 2281−2287.

(25) Tarun, J.; Huang, S.; Fukuma, Y.; Idzuchi, H.; Otani, Y.; Fukata, N.; Ishibashi, K.; Oda, S. *J. Appl. Phys.* **2011**, *109*, 07C508.

(26) Tarun, J.; Huang, S. Y.; Fukuma, Y.; Idzuchi, H.; Otani, Y.; Fukata, N.; Ishibashi, K.; Oda, S. *Appl. Phys. Express* **2012**, *5*, 045001.

(27) Liu, E. S.; Nah, J.; Varahramyan, K. M.; Tutuc, E. *Nano Lett.* **2010**, *10*, 3297−3301.

(28) Heedt, S.; Morgan, C.; Weis, K.; Bürgler, D. E.; Calarco, R.; Hardtdegen, H.; Grützmacher, D.; Schaepers, T. *Nano Lett.* **2012**, *12*, 4437−4443.

(29) Kum, H.; Heo, J.; Jahangir, S.; Banerjee, A.; Guo, W.; Bhattacharya, P. *Appl. Phys. Lett.* **2012**, *100*, 182407.

(30) DeGrave, J. P.; Schmitt, A. L.; Selinsky, R. S.; Higgins, J. M.; Keavney, D. J.; Jin, S. *Nano Lett.* **2011**, *11*, 4431−4437.

(31) Holleitner, A. W.; Sih, V.; Myers, R. C.; Gossard, A. C.; Awschalom, D. D. *Phys. Rev. Lett.* **2006**, *97*, 036805.

(32) Mal'shukov, A. G.; Chao, K. A. *Phys. Rev. B* **2000**, *61*, R2413−R2416.

(33) Tersoff, J. *Phys. Rev. Lett.* **1984**, *52*, 465−468.

(34) Rashba, E. I. *Phys. Rev. B* **2000**, *62*, R16267−R16270.

(35) Smith, D. L.; Silver, R. N. *Phys. Rev. B* **2001**, *64*, 045323.

(36) Schmidt, G.; Ferrand, D.; Molenkamp, L. W.; Filip, A. T.; van Wees, B. J. *Phys. Rev. B* **2000**, *62*, R4790−R4793.

(37) Jonsson-Akerman, B. J.; Escudero, R.; Leighton, C.; Kim, S.; Schuller, I. K.; Rabson, D. A. *Appl. Phys. Lett.* **2000**, *77*, 1870−1872.

(38) Monzon, F. G.; Patterson, D. S.; Roukes, M. L. *J. Magn. Magn. Mater.* **1999**, *195*, 19−25.

(39) van der Molen, S. J.; Tombros, N.; van Wees, B. J. *Phys. Rev. B* **2006**, *73*, 220406(R).

(40) Zwanenburg, F. A.; van der Mast, D. W.; Heersche, H. B.; Kouwenhoven, L. P.; Bakkers, E. P. A. M. *Nano Lett.* **2009**, *9*, 2704−2709.

(41) Jedema, F. J.; Heersche, H. B.; Filip, A. T.; Baselmans, J. J. A.; van Wees, B. J. *Nature* **2002**, *416*, 713−716.

(42) Johnson, M.; Silsbee, R. H. *Phys. Rev. B* **2007**, *76*, 153107.

(43) Johnson, M.; Silsbee, R. H. *Phys. Rev. Lett.* **1988**, *60*, 377.

(44) Tran, M.; Jaffres, H.; Deranlot, C.; George, J. M.; Fert, A.; Miard, A.; Lemaitre, A. *Phys. Rev. Lett.* **2009**, *102*, 036601.

(45) Chantis, A. N.; Smith, D. L. *Phys. Rev. B* **2008**, *78*, 235317.

(46) Mohite, A. D.; Perea, D. E.; Singh, S.; Dayeh, S. A.; Campbell, I. H.; Picraux, S. T.; Htoon, H. *Nano Lett.* **2012**, *12*, 1965−1971.

(47) Crooker, S. A.; Furis, M.; Lou, X.; Adelmann, C.; Smith, D. L.; Palmstrom, C. J.; Crowell, P. A. *Science* **2005**, *309*, 2191−2195.

(48) Crooker, S. A.; Garlid, E. S.; Chantis, A. N.; Smith, D. L.; Reddy, K. S. M.; Hu, Q. O.; Kondo, T.; Palmstrom, C. J.; Crowell, P. A. *Phys. Rev. B* **2009**, *80*, 041305.

(49) Valenzuela, S. O.; Monsma, D. J.; Marcus, C. M.; Narayanamurti, V.; Tinkham, M. *Phys. Rev. Lett.* **2005**, *94*, 196601.

(50) Salis, G.; Fuhrer, A.; Schlittler, R. R.; Gross, L.; Alvarado, S. F. *Phys. Rev. B* **2010**, *81*, 205323.